

Insulator-pseudogap crossover in the Lieb lattice

Kukka-Emilia Huhtinen and Päivi Törmä*

Department of Applied Physics, Aalto University, 00076 Aalto, Finland

We study the attractive Hubbard model in the Lieb lattice to understand the normal state above the superconducting critical temperature in a flat band system. We use cluster dynamical mean-field theory to compute the two-particle susceptibilities with full quantum fluctuations included in the cluster. At interaction strengths lower than the hopping amplitude, we find that the normal state on the flat band is an insulator. The insulating behavior stems from the localization properties of the flat band. A flat-band enhanced pseudogap with a depleted spectral function arises at larger interactions.

Flat, dispersionless energy bands host superconductivity governed by the quantum geometry and topology of the band [1–5]. The predicted transition temperature exceeds exponentially that of conventional superconductors [6–9], promising superconductivity at elevated temperatures. The observations of superconductivity and insulating phases at quasi-flat bands in twisted bilayer graphene [10–12] reinforce such prospects. The nature of the normal state above the critical temperature of a flat band superconductor is, however, an outstanding open question. A Fermi liquid is excluded due to the absence of a Fermi surface [13]. As the band width and kinetic energy are zero, any attractive interaction could be anticipated to cause pairing already in the normal state. Indeed preformed pairs [14, 15] and a pseudogap [16, 17] have been suggested. Here we show that the normal state in a Lieb lattice features, for decreasing interaction, a *crossover from a flat-band enhanced pseudogap to an insulator*. For small interactions, when lowering the temperature, one thus expects an insulator-superconductor transition unique to flat band systems.

The mean-field superconducting order parameter vanishes at the critical temperature. Understanding the normal state is thus inherently a beyond mean-field problem. Two-particle properties, that is, four-operator correlations must be evaluated with quantum fluctuations included. For this, we use a cluster expansion of dynamical mean-field theory (DMFT) [18]. DMFT has been used previously to investigate for example the normal state properties of the attractive single-band Hubbard model [19–21], and its cluster variants for studies of pairing fluctuations with different geometries [22]. The normal state of (partially or nearly) flat band systems with repulsive interactions has also been studied in Refs. [23–27]. We calculate the orbital-resolved pair, spin and charge susceptibilities based on two-particle Green’s functions.

We focus on the Lieb lattice, shown in Fig. 1a, due to its conceptual simplicity and experimental relevance. The localized flat band states reside at the lattice sites A

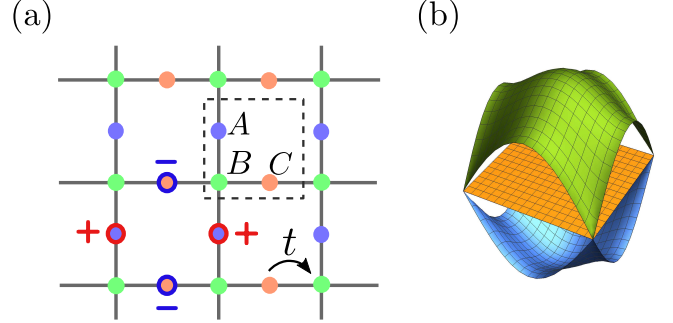


FIG. 1: (a) The Lieb lattice. The unit cell indicated with dashed lines is used as a cluster in DMFT. The three sub-lattices are labeled A , B and C as shown. An example of a localized flat band state is shown in the lower left-hand corner. The A and C sites on a square plaquette have amplitudes of alternating sign. Since we consider only nearest-neighbor hopping, this state is localized by destructive interference. (b) Band structure of the Lieb lattice. The flat band is at energy $E = 0$. On the dispersive bands, the saddle points at the edge of the Brillouin zone at energies $E = \pm 2$ lead to Van Hove singularities where the density of states also diverges.

and C only, and can be monitored separately from site B both in experiments and simulations. This gives a means of distinguishing flat band effects. The Lieb lattice has been realized experimentally for ultracold gases [28, 29], in designer lattices made by atomistic control [30, 31] and in photonic lattices [32]. Some covalent-organic frameworks are also predicted to provide the Lieb lattice [33]. We relate our predictions of the insulator and pseudogap phases to generic flat band effects to unveil their relevance beyond the Lieb lattice, for instance for moiré materials [34] where bands of different degree of flatness can be designed.

The band structure of the Lieb lattice features two dispersive bands and a perfectly dispersionless flat band,

$$E_{\pm}(\mathbf{k}) = \pm t\sqrt{2 + \cos(k_x) + \cos(k_y)}, \quad E_{\text{FB}} = 0. \quad (1)$$

where the indices $+$ and $-$ refer to the upper and lower dispersive band, respectively, FB refers to the flat band and t is the nearest-neighbor hopping amplitude. The lattice constant is taken as $a = 1$. The band structure

*Electronic address: paivi.torma@aalto.fi

is shown in Fig. 1(b). The flat band in the Lieb lattice is related to states localized due to destructive interference. An example of such a state is pictured in Fig. 1(a). Importantly, particles on the flat band occupy only the A and C sublattices.

We study the attractive Hubbard model with the Hamiltonian

$$H = \sum_{\sigma} \sum_{i\alpha, j\beta} t_{ij} c_{\sigma, i\alpha}^{\dagger} c_{\sigma, j\beta} - \sum_{\sigma} \sum_{i\alpha} \mu_{\sigma} n_{\sigma, i\alpha} \quad (2)$$

$$+ U \sum_{i\alpha} (n_{\uparrow, i\alpha} - 1/2)(n_{\downarrow, i\alpha} - 1/2), \quad (3)$$

where $c_{\sigma, i\alpha}^{\dagger}$ is the creation operator for a fermion with spin $\sigma = \uparrow, \downarrow$ in the unit cell i and the sublattice $\alpha = A, B, C$ and $n_{\sigma, i\alpha} = c_{\sigma, i\alpha}^{\dagger} c_{\sigma, i\alpha}$. The hopping amplitude t_{ij} is 1 between connected sites and 0 otherwise; below, all energies are thus in units of the hopping t . The on-site interaction strength is denoted by U .

To study normal state properties, we use a cluster expansions of DMFT where we use one unit cell of the Lieb lattice as our cluster (see Fig. 1a). In this method, the lattice model is mapped to an effective Anderson impurity model, and the lattice quantities are computed self-consistently. The self-energy is assumed to be uniform and local to each unit cell, $\Sigma_{ij} \approx \Sigma \delta_{ij}$. Here, Σ is a matrix in the orbital indices.

More precisely, the principle of dynamical mean-field theory is as follows. The self-energy $\Sigma(i\omega_n)$ and Green's function $G(\mathbf{k}, i\omega_n)$ are related by the Dyson equation

$$G(\mathbf{k}, i\omega_n) = [G^0(\mathbf{k}, i\omega_n)^{-1} - \Sigma(i\omega_n)]^{-1}, \quad (4)$$

where $G^0(\mathbf{k}, i\omega_n)$ is the non-interacting Green's function and ω_n are fermionic Matsubara frequencies. To map the lattice model to an impurity model, we consider the local part of the Green's function $\overline{G}(i\omega_n) = \sum_{\mathbf{k}} G(i\omega_n, \mathbf{k})$. The bath Green's function of the impurity model is obtained from

$$\mathcal{G}^0(i\omega_n) = [\overline{G}^{-1}(i\omega_n) + \Sigma(i\omega_n)]^{-1}. \quad (5)$$

In this work, the impurity problem defined by $\mathcal{G}^0(i\omega_n)$ is solved using an interaction expansion continuous time Monte Carlo solver (CT-INT) [35, 36]. The solution of the impurity problem provides the impurity Green's function $\mathcal{G}(i\omega_n)$ and a new estimate for the self-energy. In DMFT, the self-energy of the impurity is equal to the self-energy of the lattice, so the result can be plugged into Eq. (4). This procedure is repeated until the self-consistency condition $\overline{G}(i\omega_n) = \mathcal{G}(i\omega_n)$ is fulfilled.

Calculation of the two-particle susceptibilities is a central and highly non-trivial part of our work. The main ideas are discussed here, and further details are given in the supplementary material [37]. This procedure [38] allows to compute the generalized susceptibilities

$$\chi_{ijkl}(\tau_1, \tau_2, \tau_3) = G_{ijkl}^{(4)}(\tau_1, \tau_2, \tau_3) - G_{ij}(\tau_1, \tau_2)G_{kl}(\tau_3, 0), \quad (6)$$

where $G_{ijkl}^{(4), \text{ph}}(\tau_1, \tau_2, \tau_3) = \langle T_{\tau} [c_i^{\dagger}(\tau_1) c_j(\tau_2) c_k^{\dagger}(\tau_3) c_l(0)] \rangle$ is the two-particle Green's function. Here, T_{τ} is the imaginary time ordering operator and τ_i are imaginary times. The indices i, j, k, l contain the spin and the orbital indices A, B or C . To conveniently define the spin, charge and pairing susceptibilities, we define the Fourier transform in the particle-hole (ph) and particle-particle (pp) channels as follows:

$$\chi_{ijkl}^{\text{ph}, \omega, \omega', \nu} = \int_0^{\beta} \int_0^{\beta} \int_0^{\beta} d\tau_1 d\tau_2 d\tau_3 \chi_{ijkl}(\tau_1, \tau_2, \tau_3) e^{-i\omega\tau_1} e^{i(\nu+\omega)\tau_2} e^{-i(\nu+\omega')\tau_3}, \quad (7)$$

$$\chi_{ijkl}^{\text{pp}, \omega, \omega', \nu} = \int_0^{\beta} \int_0^{\beta} \int_0^{\beta} d\tau_1 d\tau_2 d\tau_3 \chi_{ijkl}(\tau_1, \tau_2, \tau_3) e^{-i\omega\tau_1} e^{i(\nu-\omega')\tau_2} e^{-i(\nu-\omega)\tau_3}, \quad (8)$$

where ν is a bosonic Matsubara frequency and ω and ω' are fermionic Matsubara frequencies. Both χ^{pp} and χ^{ph} contain the same information.

The generalized susceptibilities can be computed with the impurity solver for the cluster. However, within DMFT, the local cluster susceptibilities are not equal to the lattice susceptibilities. Instead, the self-consistency is only at the level of the local irreducible vertex function Γ , which is the two-particle equivalent to the self-energy. Like the self-energy, the irreducible vertex is assumed to be momentum-independent. It is related to the generalized susceptibilities by the Bethe-Salpeter equation

$$\chi_{ijkl}^{c, \omega, \omega', \nu} = \chi_{0,ijkl}^{c, \omega, \omega', \nu} + \chi_{0,ij'j'i'}^{c, \omega, \omega'', \nu} \Gamma_{i'j'k'l'}^{c, \omega'', \omega''', \nu} \chi_{k'l'l}^{c, \omega''', \omega', \nu}. \quad (9)$$

Here, c denotes the channel and χ_0^c is the bare susceptibility, for example in the particle-hole channel $\chi_{0,ijkl}^{\text{ph}, \omega, \omega', \nu} = -\beta \delta_{\omega, \omega'} G_{il}(i\omega) G_{kj}(i(\omega + \nu))$. Repeated indices are summed over. The Bethe-Salpeter equation can be written separately for the local cluster quantities and the lattice quantities. The irreducible vertex in each channel is obtained by inverting the Bethe-Salpeter equation for the impurity quantities. Within DMFT, the irreducible vertex of the impurity is equal to that of the lattice, so the lattice susceptibilities can then be computed by plugging the result in the Bethe-Salpeter equation for the lattice quantities.

We first study the local contributions to the static spin susceptibility, given by

$$\chi_{\alpha}^{\text{spin}} = \frac{1}{\beta^2} \sum_{\omega, \omega'} \left(\chi_{\uparrow\alpha, \uparrow\alpha, \uparrow\alpha, \uparrow\alpha}^{\text{ph}, \omega, \omega', \nu=0} - \chi_{\uparrow\alpha, \uparrow\alpha, \downarrow\alpha, \downarrow\alpha}^{\text{ph}, \omega, \omega', \nu=0} \right). \quad (10)$$

These susceptibilities are shown in Fig. 2(a) at half filling $\mu = 0$. The susceptibility at the B site increases monotonously when the temperature is lowered. This is

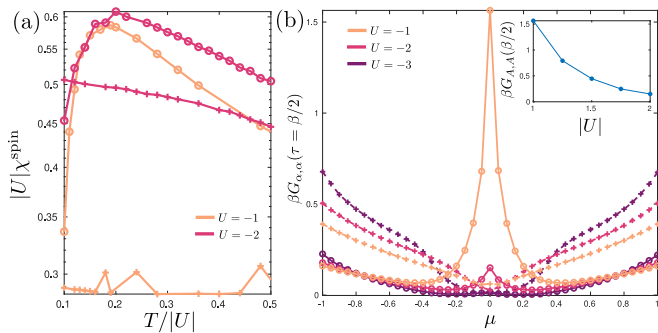


FIG. 2: (a) Orbital-resolved spin susceptibilities $\chi_\alpha^{\text{spin}}$ as a function of $T/|U|$ at half-filling for interaction strengths $U = -1$ and $U = -2$. The susceptibilities are multiplied by the interaction strength for visual clarity. In both (a) and (b), results for the A site are plotted with circles and results for the B site with crosses. The flat band states are located only on the A/C sites. (b) The Green's function $\beta G_{\alpha,\alpha}(\tau = \beta/2)$ at inverse temperature $\beta = 20$ as a function of chemical potential μ . Pairing is suppressed so that the superconducting transition does not take place. The inset shows $\beta G_{A,A}(\beta/2)$ at half-filling $\mu = 0$ at different interaction strengths. The results for the A and C sites are identical due to the symmetry of the Lieb lattice.

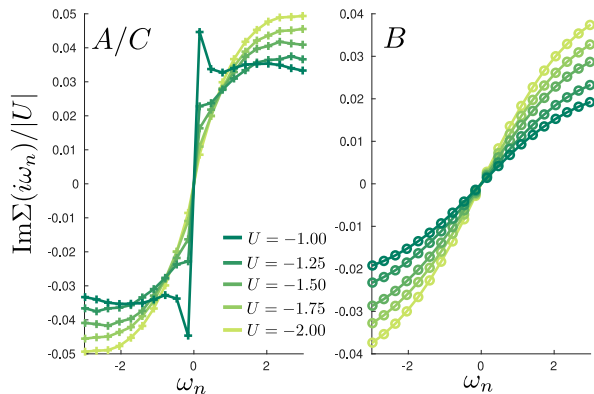


FIG. 3: Imaginary part of the self-energy at half-filling and inverse temperature $\beta = 20$. The superconducting order is suppressed. The left panel shows the divergence of the self-energy, a signature of a non-Fermi liquid insulator, at low interactions on the A/C sites. The right panel shows the behavior at the B site, which is the one expected for a Fermi liquid.

consistent with Fermi liquid behavior. On the A/C sites at both $U = -1$ and $U = -2$, the spin susceptibility increases down to $T \approx 0.2|U|$, at which point it decreases rapidly. This indicates a pseudogap at the A/C sites. We find this pseudogap also away from the flat band, as discussed in [37].

To get further information about the nature of the normal state, we study the Green's functions in the middle of the imaginary time interval, $G_{\alpha\alpha}(\beta/2)$. This quantity is related to the orbital-resolved local spectral function

\mathcal{A}_α by [39, 40]

$$\beta G_{\alpha\alpha}(\beta/2) = \int \frac{d\omega}{2\pi T} \frac{\mathcal{A}_\alpha(\omega)}{\cosh[\omega/(2T)]}. \quad (11)$$

Since the integral is dominated by the range $\omega \leq T$, $\beta G_{\alpha\alpha}(\beta/2)$ approximates $\mathcal{A}_i(\omega = 0)$ at low temperatures. The advantage of studying $\beta G_{\alpha\alpha}(\beta/2)$ is that it avoids the analytical continuation necessary to obtain the spectral function within DMFT. However, since $\beta G_{\alpha\alpha}(\beta/2)$ is only a reasonable approximation for the spectral function at low temperatures, its study requires a suppression of the superconducting order so that the phase transition is avoided. Regardless, it provides us with qualitative information about the nature of the normal state.

In a Fermi liquid at zero temperature, the spectral function becomes the orbital resolved non-interacting density of states ρ_α , evaluated at chemical potential shifted by the self-energy $\mathcal{A}_\alpha = \rho_\alpha(\mu - \text{Re}\Sigma(\omega = 0))$. In the Lieb lattice, the non-interacting density of states at the A/C sites is infinite at $\mu = 0$ due to the flat band. As can be seen from Fig. 2(b), this feature is not present in the spectral function at large interactions. For low interaction strengths, a peak in $\beta G_{AA}(\beta/2)$ is still visible, but when the interaction is increased, $\beta G_{AA}(\beta/2)$ becomes depleted in an increasingly wide region. This confirms the non-Fermi liquid behavior in the spin susceptibility at the A/C in Fig. 2(a) is indeed related to a pseudogap in the normal state.

While the spectral function tells about a pseudogap, at low interactions, the imaginary part of the self-energy is helpful in characterizing the flat band normal state. In a Fermi liquid, $\text{Im}\Sigma(i\omega_n)$ vanishes linearly at low frequencies, $\text{Im}\Sigma(i\omega_n) \approx i\omega_n a + b$. As shown in Fig. 3, this is observed at the B site. At a low interaction $U = -1$, $\text{Im}\Sigma_{A/C}(\omega)$ instead seems to diverge at $\omega = 0$. As the interaction strength is increased, the divergence at $\omega = 0$ disappears and the linear behavior expected for a Fermi liquid is recovered around $U \approx -1.75$. The imaginary part of the self-energy is related to the quasiparticle weight Z by

$$Z = \left(1 - \frac{\text{Im}\Sigma(i\omega_n)}{\omega_n} \Big|_{\omega_n \rightarrow 0} \right)^{-1}. \quad (12)$$

Due to the momentum-independence of the self-energy within DMFT, $Z = m/m^*$, where m is the bare mass and m^* is the effective mass [41]. The divergence of $\text{Im}\Sigma(i\omega_n)$ around $\omega = 0$ thus indicates a divergence of the effective mass. Therefore, at low interaction strengths, the divergence in the self-energy at zero frequency indicates insulating behavior.

The results we present for the self-energy are at a low temperature with the superconducting order suppressed. This is necessary because the zero frequency is not accessible on the discrete fermionic Matsubara frequency

scale. At high temperatures, we observe the diverging behavior in the self-energy already at higher interaction strengths, but this is likely an artifact of the discrete frequency scale: $\text{Im}\Sigma(i\omega_n)$ vanishes so fast at $\omega = 0$ that the linear regime is entirely below the lowest Matsubara frequency. The diverging behavior in the self-energy at $U = -1$ and below subsists to very low temperatures, indicating an insulating state as opposed to a metal with very high quasiparticle effective mass.

We thus find two different non-Fermi liquid phases in the normal state. When the hopping amplitude is of the order of the interaction or larger, the self-energy at the A/C sites diverges at $\omega = 0$, indicating insulating behavior related to the flat band. When the interaction is increased, the insulating behavior disappears as shown by Fig. 3(a), and the spectral function is increasingly suppressed at low temperatures (Fig. 2(a)). This is a pseudogap phase. The spin susceptibility (Fig. 2(a)) shows non-Fermi liquid features indicating a pseudogap even at interaction $U = -1$, suggesting the pseudogap and insulator can coexist. However, the onset temperature of the pseudogap becomes vanishingly close to the superconducting critical temperature at low interaction strengths. In both the insulator and pseudogap cases, the non-Fermi liquid around half-filling is linked to the flat band, and the behavior at the B site is that of a Fermi liquid.

A pseudogap was also predicted in the normal state of the Lieb lattice in [16]. In this Monte Carlo study, a metallic state is predicted at low interaction strengths and a pseudogap phase with short range pairing correlations at intermediate interactions. In contrast, our results show that the state at low interaction strengths at the flat band singularity is not a metallic Fermi liquid phase, but rather an insulator. In agreement with this previous study, we find that the normal state at interactions above $|U| \approx 1$ is a pseudogap phase, characterized here by a depletion of the spectral function and a suppressed spin susceptibility. A similar pseudogap state was predicted in [17] for a lattice model with a quasi-flat band. The onset temperature of the pseudogap in that study is predicted to be almost proportional to the interaction strength, which is similar to our result. In summary, the pseudogap is consistent with previous literature, but the insulator we predict at low interactions has not been found before.

In presence of singularities such as van Hove or flat band ones, it is particularly important to compare competing ordered phases. To this extent, we study the pairing and charge susceptibilities, given by

$$\chi_{\alpha}^{\text{pair}} = \frac{1}{\beta^2} \sum_{\omega, \omega'} \chi_{\uparrow\alpha, \uparrow\alpha, \downarrow\alpha, \downarrow\alpha}^{\text{pp}, \omega, \omega', \nu=0} \quad (13)$$

$$\chi_{\alpha}^{\text{charge}} = \frac{1}{\beta^2} \sum_{\omega, \omega'} \left(\chi_{\uparrow\alpha, \uparrow\alpha, \uparrow\alpha, \uparrow\alpha}^{\text{ph}, \omega, \omega', \nu=0} + \chi_{\uparrow\alpha, \uparrow\alpha, \downarrow\alpha, \downarrow\alpha}^{\text{ph}, \omega, \omega', \nu=0} \right). \quad (14)$$

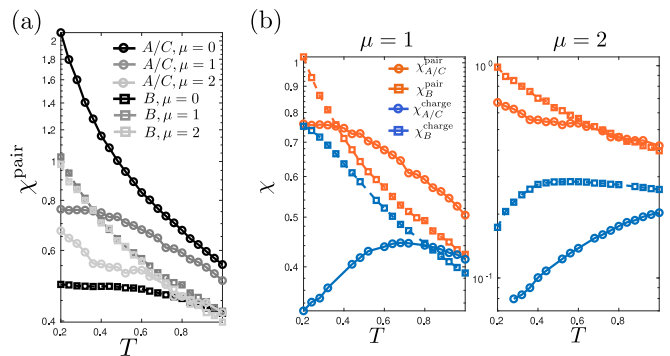


FIG. 4: (a) Pairing susceptibilities $\chi_{\alpha}^{\text{pair}}$ as a function of temperature for different chemical potentials. (b) Pairing and charge susceptibilities at $\mu = 1$ (left panel) and $\mu = 2$ (right panel) as a function of temperature. The legend for the right panel is the same as for the left. The interaction strength for all figures is $U = -2$.

The pairing susceptibilities at $U = -2$ and different chemical potentials are shown in Fig. 4(a). At half-filling $\mu = 0$, when the flat band is occupied, the pairing susceptibility is strongly dominated by the A/C sites, where the flat band states reside. On the other hand, the pairing susceptibility χ_B^{pair} barely increases below $T \approx 0.6$. The total pairing susceptibility diverges at the critical temperature $T_C \approx 0.11$, so this shows that the phase transition is driven by pairing at the A/C sites. When the chemical potential is tuned away from the flat band, the susceptibility at the B site becomes the dominant susceptibility. The difference between the susceptibilities in the different sublattices is however not as pronounced as at the flat band.

The total pairing susceptibility diverges as the critical temperature is approached at all chemical potentials. However, even accounting for the different critical temperatures, the pairing susceptibility at the flat band singularity is always larger than the local pairing susceptibilities away from the flat band. The large difference between the susceptibilities at the A/C and B sites at $\mu = 0$ is thus not only due to a suppression of the susceptibility at the B site, but the flat band enhances the local pairing susceptibility at the A/C sites.

An important question is whether the charge susceptibility overtakes the pairing susceptibility. At half-filling, the pairing and charge susceptibilities are equal due to the symmetry of the system. Charge susceptibilities for $\mu = 1$ and $\mu = 2$ are shown in Fig. 4(b). At $\mu = 1$, the charge susceptibility at the A/C sites is suppressed, but χ_B^{charge} quite close to the pairing susceptibility on the B site. At low temperatures, however, the pairing susceptibility grows faster than the charge susceptibility, so superconductivity is the leading instability. At $\mu = 2$, the charge susceptibility is suppressed at all lattice sites. It should be noted that the Van Hove singularity in the Lieb lattice is not at half filling, contrary to the square

lattice, hence the pairing and charge susceptibilities are not equal at the Van Hove singularity.

In summary, we found a crossover between two non-Fermi liquid normal states in the Lieb lattice: an insulator at the A/C sites below interactions of $|U| \simeq 1$ and a metallic state featuring a pseudogap above. The insulator and pseudogap can coexist in a small temperature range. We confirmed that pairing is the leading instability. The crossover can be observed in present-day ultracold gas setups since cooling below the critical temperature, often an obstacle, is not needed, and susceptibilities [42] and pseudogaps [43, 44] can be measured. In twisted bilayer graphene (TBG) the interaction strength is not known, but mean-field studies indicate it is in the regime where flat band effects are significant [5, 45–47]. Thus the possibility of a flat-band insulator interacting normal state should be considered in addition to pseudogap [48] and other exotic normal states [49, 50] already observed, in particular for other moiré materials with stronger flat band character than TBG. Due to the particle-hole symmetry, our results are also relevant for flat band magnetism [51–53]: the spin susceptibility maps to the charge susceptibility and *vice versa*.

Pseudogap phases have been predicted and observed in many strongly interacting dispersive systems [20, 44, 54, 55]. For instance in the square lattice with attractive interactions it appears for large interactions while the weak interaction regime is a Fermi-liquid [20]. Here we showed that a flat band enhances the pseudogap formation. The insulator behavior found at small interactions is qualitatively unique to flat bands. Insulator-superconductor phase transitions are ubiquitous, controlled by for instance the magnetic field [56–58], disorder [59–61], or doping [62–64]. Here, the insulator-superconductor transition originates from geometry-induced localization of single particles in a flat band.

Acknowledgments— We thank Pramod Kumar for useful discussions. We acknowledge support by the Academy of Finland under project numbers 303351, 307419, and 327293. Kukka-Emilia Huhtinen acknowledges financial support by the Magnus Ehrnrooth Foundation. Computing resources were provided by CSC – the Finnish IT Centre for Science.

[1] S. Peotta and P. Törmä, *Nat. Comm.* **6**, 8944 (2015).
 [2] A. Julku, S. Peotta, T. I. Vanhala, D.-H. Kim, and P. Törmä, *Phys. Rev. Lett.* **117**, 045303 (2016).
 [3] L. Liang, T. I. Vanhala, S. Peotta, T. Siro, A. Harju, and P. Törmä, *Phys. Rev. B* **95**, 024515 (2017).
 [4] T. Hazra, N. Verma, and M. Randeria, *Phys. Rev. X* **9**, 031049 (2019).
 [5] F. Xie, Z. Song, B. Lian, and B. A. Bernevig, *Phys. Rev. Lett.* **124**, 167002 (2020).
 [6] V. A. Khodel and V. R. Shaginyan, *JETP* **51**, 553 (1990).

[7] V. Khodel, V. Shaginyan, and V. Khodel, *Physics Reports* **249**, 1 (1994).
 [8] T. T. Heikkilä, N. B. Kopnin, and G. E. Volovik, *JETP Letters* **94**, 233 (2011).
 [9] N. B. Kopnin, T. T. Heikkilä, and G. E. Volovik, *Phys. Rev. B* **83**, 220503(R) (2011).
 [10] Y. Cao, V. Fatemi, A. Demir, S. Fang, S. L. Tomarken, J. Y. Luo, J. D. Sanchez-Yamagishi, K. Watanabe, T. Taniguchi, E. Kaxiras, R. C. Ashoori, and P. Jarillo-Herrero, *Nature* **556** (2018).
 [11] Y. Cao, V. Fatemi, S. Fang, K. Watanabe, T. Taniguchi, E. Kaxiras, and P. Jarillo-Herrero, *Nature* **556** (2018).
 [12] M. Yankowitz, S. Chen, H. Polshyn, Y. Zhang, K. Watanabe, T. Taniguchi, D. Graf, A. F. Young, and C. R. Dean, *Science* **363**, 1059 (2019).
 [13] P. Gurin and Z. Gulácsi, *Phys. Rev. B* **64**, 045118 (2001).
 [14] M. Tovmasyan, S. Peotta, L. Liang, P. Törmä, and S. D. Huber, *Phys. Rev. B* **98**, 134513 (2018).
 [15] P. Törmä, L. Liang, and S. Peotta, *Phys. Rev. B* **98**, 220511(R) (2018).
 [16] N. Swain and M. Karmakar, *Phys. Rev. Research* **2**, 023136 (2020).
 [17] J. S. Hofmann, E. Berg, and D. Chowdhury, arXiv e-prints, arXiv:1912.08848 (2019), arXiv:1912.08848 .
 [18] T. A. Maier, M. Jarrell, T. Pruschke, and M. Hettler, *Rev. Mod. Phys.* **77**, 1027 (2005).
 [19] M. Capone, C. Castellani, and M. Grilli, *Phys. Rev. Lett.* **88**, 126403 (2002).
 [20] M. Keller, W. Metzner, and U. Schollwöck, *Phys. Rev. Lett.* **86**, 4612 (2001).
 [21] A. Toschi, P. Barone, M. Capone, and C. Castellani, *New Journal of Physics* **7**, 7 (2005).
 [22] X. Chen, J. P. F. LeBlanc, and E. Gull, *Phys. Rev. Lett.* **115**, 116402 (2015).
 [23] H. Shinaoka, S. Hoshino, M. Troyer, and P. Werner, *Phys. Rev. Lett.* **115**, 156401 (2015).
 [24] P. Kumar, T. I. Vanhala, and P. Törmä, *Phys. Rev. B* **100**, 125141 (2019).
 [25] P. Kumar, S. Peotta, Y. Takasu, Y. Takahashi, and P. Törmä, arXiv e-prints, arXiv:2005.05457 (2020), arXiv:2005.05457 .
 [26] E. W. Huang, M.-S. Vaezi, Z. Nussinov, and A. Vaezi, *Phys. Rev. B* **99**, 235128 (2019).
 [27] S. Sayyad, E. W. Huang, M. Kitatani, M.-S. Vaezi, Z. Nussinov, A. Vaezi, and H. Aoki, *Phys. Rev. B* **101**, 014501 (2020).
 [28] S. Taie, H. Ozawa, T. Ichinose, T. Nishio, S. Nakajima, and Y. Takahashi, *Science Advances* **1** (2015), 10.1126/sciadv.1500854.
 [29] H. Ozawa, S. Taie, T. Ichinose, and Y. Takahashi, *Phys. Rev. Lett.* **118**, 175301 (2017).
 [30] M. R. Slot, T. S. Gardenier, P. H. Jacobse, G. C. P. van Miert, S. N. Kempkes, S. J. M. Zevenhuizen, C. M. Smith, D. Vanmaekelbergh, and I. Swart, *Nat Phys* **13**, 672 (2017).
 [31] R. Drost, T. Ojanen, A. Harju, and P. Liljeroth, *Nat Phys* **13**, 668 (2017).
 [32] S. Mukherjee, A. Spracklen, D. Choudhury, N. Goldman, P. Öhberg, E. Andersson, and R. R. Thomson, *Phys. Rev. Lett.* **114**, 245504 (2015).
 [33] B. Cui, X. Zheng, J. Wang, D. Liu, S. Xie, and B. Huang, *Nat. Comm.* **11**, 66 (2020).
 [34] L. Balents, C. R. Dean, D. K. Efetov, and A. F. Young,

- Nature Physics* **16**, 725 (2020).
- [35] F. F. Assaad and T. C. Lang, *Phys. Rev. B* **76**, 035116 (2007).
- [36] E. Gull, A. J. Millis, A. I. Lichtenstein, A. N. Rubtsov, M. Troyer, and P. Werner, *Rev. Mod. Phys.* **83**, 349 (2011).
- [37] See Supplemental Material for details on the method to compute generalized susceptibilities within DMFT and discussion of pseudogap behaviour away from the flat band.
- [38] G. Rohringer, A. Valli, and A. Toschi, *Phys. Rev. B* **86**, 125114 (2012).
- [39] E. Gull, O. Parcollet, P. Werner, and A. J. Millis, *Phys. Rev. B* **80**, 245102 (2009).
- [40] N. Trivedi and M. Randeria, *Phys. Rev. Lett.* **75**, 312 (1995).
- [41] E. Müller-Hartmann, *International Journal of Modern Physics B* **03**, 2169 (1989), <https://doi.org/10.1142/S0217979289001391>.
- [42] J. Meineke, J.-P. Brantut, D. Stadler, T. Müller, H. Moritz, and T. Esslinger, *Nature Physics* **8**, 454 (2012).
- [43] J. P. Gaebler, J. T. Stewart, T. E. Drake, D. S. Jin, A. Perali, P. Pieri, and G. C. Strinati, *Nature Physics* **6**, 569 (2010).
- [44] M. Feld, B. Fröhlich, E. Vogt, M. Koschorreck, and M. Köhl, *Nature* **480**, 75 (2011).
- [45] A. Julku, T. J. Peltonen, L. Liang, T. T. Heikkilä, and P. Törmä, *Phys. Rev. B* **101**, 060505(R) (2020).
- [46] X. Hu, T. Hyart, D. I. Pikulin, and E. Rossi, *Phys. Rev. Lett.* **123**, 237002 (2019).
- [47] L. Classen, *Physics* **13** (2020), 10.1103/Physics.13.23.
- [48] Y. Jiang, X. Lai, K. Watanabe, T. Taniguchi, K. Haule, J. Mao, and E. Y. Andrei, *Nature* **573**, 91 (2019).
- [49] U. Zondiner, A. Rozen, D. Rodan-Legrain, Y. Cao, R. Queiroz, T. Taniguchi, K. Watanabe, Y. Oreg, F. von Oppen, A. Stern, E. Berg, P. Jarillo-Herrero, and S. Ilani, *Nature* **582**, 203 (2020).
- [50] D. Wong, K. P. Nuckolls, M. Oh, B. Lian, Y. Xie, S. Jeon, K. Watanabe, T. Taniguchi, B. A. Bernevig, and A. Yazdani, *Nature* **582**, 198 (2020).
- [51] A. Mielke, *Journal of Physics A: Mathematical and General* **25**, 4335 (1992).
- [52] H. Tasaki, *Phys. Rev. Lett.* **69**, 1608 (1992).
- [53] A. Mielke and H. Tasaki, *Comm. Math. Phys.* **158**, 341 (1993).
- [54] C. Huscroft, M. Jarrell, T. Maier, S. Moukouri, and A. N. Tahvildarzadeh, *Phys. Rev. Lett.* **86**, 139 (2001).
- [55] E. Gull, O. Parcollet, and A. J. Millis, *Phys. Rev. Lett.* **110**, 216405 (2013).
- [56] A. Yazdani and A. Kapitulnik, *Phys. Rev. Lett.* **74**, 3037 (1995).
- [57] N. Hadacek, M. Sanquer, and J.-C. Villégier, *Phys. Rev. B* **69**, 024505 (2004).
- [58] T. I. Baturina, C. Strunk, M. R. Baklanov, and A. Satta, *Phys. Rev. Lett.* **98**, 127003 (2007).
- [59] R. W. Crane, N. P. Armitage, A. Johansson, G. Sambandamurthy, D. Shahar, and G. Grüner, *Phys. Rev. B* **75**, 094506 (2007).
- [60] B. Sacépé, T. Dubouchet, C. Chapelier, M. Sanquer, M. Ovia, D. Shahar, M. Feigel'man, and L. Ioffe, *Nature Physics* **7**, 239 (2011).
- [61] G.-H. Lee, D. Jeong, K.-S. Park, Y. Meir, M.-C. Cha, and H.-J. Lee, *Scientific Reports* **5**, 13466 (2015).
- [62] K. Semba and A. Matsuda, *Phys. Rev. Lett.* **86**, 496 (2001).
- [63] Z. Konstantinovi, Z. Li, and H. Raffy, *Physica C: Superconductivity* **351**, 163 (2001).
- [64] S. Oh, T. A. Crane, D. J. Van Harlingen, and J. N. Eckstein, *Phys. Rev. Lett.* **96**, 107003 (2006).

Supplementary material: Insulator-pseudogap crossover in the Lieb lattice

Kukka-Emilia Huhtinen and Päivi Törmä*
Department of Applied Physics, Aalto University, 00076 Aalto, Finland

COMPUTATION OF TWO-PARTICLE QUANTITIES WITHIN DMFT

The two-particle Green's function is defined as

$$G_{ijkl}^{(4),\text{ph}}(\tau_1, \tau_2, \tau_3) = \left\langle T_\tau [c_i^\dagger(\tau_1) c_j(\tau_2) c_k^\dagger(\tau_3) c_l(0)] \right\rangle. \quad (\text{S1})$$

Here, T_τ is the imaginary time ordering operator and τ_i are imaginary times. The indices i, j, k, l contain the spin and the orbital A, B or C . Of particular interest is the generalized susceptibility

$$\chi_{ijkl}(\tau_1, \tau_2, \tau_3) = G_{ijkl}^{(4)}(\tau_1, \tau_2, \tau_3) - G_{ij}(\tau_1, \tau_2) G_{kl}(\tau_3, 0). \quad (\text{S2})$$

We define the Fourier transform of the generalized susceptibility in the particle-hole (ph) and particle-particle (pp) channels as follows:

$$\chi_{ijkl}^{\text{ph},\omega,\omega',\nu} = \int_0^\beta \int_0^\beta \int_0^\beta d\tau_1 d\tau_2 d\tau_3 \chi_{ijkl}(\tau_1, \tau_2, \tau_3) e^{-i\omega\tau_1} e^{i(\nu+\omega)\tau_2} e^{-i(\nu+\omega')\tau_3}, \quad (\text{S3})$$

$$\chi_{ijkl}^{\text{pp},\omega,\omega',\nu} = \int_0^\beta \int_0^\beta \int_0^\beta d\tau_1 d\tau_2 d\tau_3 \chi_{ijkl}(\tau_1, \tau_2, \tau_3) e^{-i\omega\tau_1} e^{i(\nu-\omega')\tau_2} e^{-i(\nu-\omega)\tau_3}. \quad (\text{S4})$$

Both χ^{pp} and χ^{ph} contain the same information, but these definitions allow to conveniently define the charge and pairing susceptibilities.

The generalized susceptibilities can be solved with the impurity solver for the cluster. However, within DMFT, the impurity susceptibilities are not equal to the lattice susceptibilities. Instead, the self-consistency is only at the level of the local irreducible vertex function Γ . The irreducible vertex is the two-particle equivalent to the self-energy. The self-energy is the sum of all irreducible diagrams connecting two external legs. The irreducible vertex is the sum of all irreducible diagrams connecting four external legs. However, the reducibility of a graph depends on the channel, as there are several possible ways to disconnect pairs of outer legs. Thus the irreducible vertex is channel-dependent.

*Electronic address: paivi.torma@aalto.fi

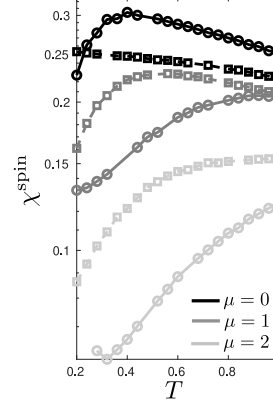


FIG. S1: Spin susceptibility as a function of temperature for different chemical potentials. The interaction strength is $U = -2$. The susceptibility at the A/C sites is plotted with dots, and the susceptibility at the B site is plotted with squares.

The irreducible vertex is related to the generalized susceptibility by the Bethe-Salpeter equation :

$$\chi_{ijkl}^{c,\omega,\omega',\nu}(\mathbf{k}, \mathbf{k}', \mathbf{q}) = \chi_0^{c,\omega,\omega',\nu}(\mathbf{k}, \mathbf{k}', \mathbf{q}) + \chi_0^{c,\omega,\omega'',\nu}(\mathbf{k}, \mathbf{k}_1, \mathbf{q}) \Gamma_{i'j'k'l'}^{c,\omega'',\omega''',\nu}(\mathbf{k}_1, \mathbf{k}_2, \mathbf{q}) \chi_{k'l'l}^{c,\omega''',\omega',\nu}(\mathbf{k}_2, \mathbf{k}', \mathbf{q}). \quad (\text{S5})$$

where repeated indices are summed over and c denotes the channel. Here χ_0^c is the bare contribution to the susceptibility, for example in the particle-hole channel $\chi_0^{\text{ph},\omega,\omega',\nu}(\mathbf{k}, \mathbf{k}', \mathbf{q}) = -\beta \delta_{\omega,\omega'} \delta_{\mathbf{k},\mathbf{k}'} G_{il}(\omega, \mathbf{k}) G_{kj}(\omega + \nu, \mathbf{k} + \mathbf{q})$.

In DMFT, the vertex $\Gamma(\mathbf{q}, \mathbf{k}, \mathbf{k}')$ is approximated by the local vertex Γ of the impurity. Summing over the momenta \mathbf{k} and \mathbf{k}' , we obtain

$$\chi_{ijkl}^{c,\omega,\omega',\nu}(\mathbf{q}) = \chi_0^{c,\omega,\omega',\nu}(\mathbf{q}) + \chi_0^{c,\omega,\omega'',\nu}(\mathbf{q}) \Gamma_{i'j'k'l'}^{c,\omega'',\omega''',\nu} \chi_{k'l'l}^{c,\omega''',\omega',\nu}(\mathbf{q}). \quad (\text{S6})$$

This equation can be written separately for the lattice quantities and the impurity quantities χ_{imp} and $\chi_{0,\text{imp}}$. For the impurity, we further approximate the susceptibilities by the local ones, so that

$$\chi_{\text{imp},ijkl}^{c,\omega,\omega',\nu} = \chi_{0,\text{imp},ijkl}^{c,\omega,\omega',\nu} + \chi_{0,\text{imp},ij'j'i'}^{c,\omega,\omega'',\nu} \Gamma_{i'j'k'l'}^{c,\omega'',\omega''',\nu} \chi_{\text{imp},k'l'l}^{c,\omega''',\omega',\nu}. \quad (\text{S7})$$

The local vertex is computed by inverting this equation. Since within DMFT it is the same as the vertex of the

lattice, the lattice susceptibility can be computed by substituting the result in the Bethe-Salpeter equation for the lattice model. In matrix form, the result can be written

$$[\chi(i\nu, \mathbf{q})]^{-1} = [\chi_0(i\nu, \mathbf{q})]^{-1} - [\chi_{0,\text{imp}}(i\nu)]^{-1} + [\chi_{\text{imp}}(i\nu)]^{-1}. \quad (\text{S8})$$

Here the matrices representing the susceptibilities at each $i\nu$ are block matrices in the two fermionic Matsubara frequencies ω, ω' .

PSEUDOGAP AWAY FROM HALF-FILLING

Figure S1 shows the local spin susceptibilities at different chemical potentials. The non-Fermi liquid behavior

found only at the A/C sites on the flat band is found at all sites when the chemical potential is tuned away from the flat band. A pseudogap phase thus occurs also away from the flat band, but a qualitative difference in the behavior at the A/C sites and the B site is only found at the flat band.